Phys. Lett. B 881 (2026) 140892

Contents lists available at ScienceDirect

Physics Letters B

journal homepage: www.elsevier.com/locate/physletb

Letter

Kinematic constraint on the residue phase in elastic resonances

S. Ceci [a,*], R. Omerović [b], H. Osmanović [b], M. Uroić [a], M. Vukšić [c], B. Zauner [d]

[a] Rudjer Bošković Institute, Bijenička 54, HR-10000, Zagreb, Croatia
[b] University of Tuzla, Urfeta Vejzagića 4, Tuzla, 75000, Bosnia and Herzegovina
[c] University of Oxford, Oxford OX1 2JD, United Kingdom
[d] Institute for Medical Research and Occupational Health, Ksaverska 2, Zagreb, HR-10000, Croatia

ARTICLE INFO

Editor: Feng Bo

PACS:
14.40.Be
14.40.Df
14.20.Gk
11.55.Bq

Keywords:
Light non-strange mesons
Light strange mesons
Nucleon resonances
Analytic properties of S matrix

ABSTRACT

We show that the complex-plane structure of light hadron resonances is governed by a unified kinematic framework where the threshold position plays a decisive role. By applying this framework to $\pi\pi$, πK, and πN phase shifts, we show that the residue phase θ is primarily determined by the threshold-locked phase δ_0 (the angle between pole and real axis seen from the threshold). While vector resonances exhibit excellent alignment with this kinematic baseline, scalar resonances show systematic deviations of 10°–15°, which we identify as the uncompensated residual of subthreshold chiral dynamics.

1. Introduction

Resonances are fundamentally defined as simple poles of the S-matrix on non-physical Riemann sheets [1]. While the real and imaginary parts of the pole position are the resonance mass M and total width Γ, and the residue magnitude defines the coupling strength, the physical origin of the residue phase θ has remained elusive [2]. Traditionally attributed to background interference and coupling phases, recent findings suggest that for the lightest resonances, S-matrix unitarity constrains θ to a fundamental kinematic identity [3,4].

In this Letter, we use this constraint to resolve the complex-plane structure of the lightest scalar and vector mesons. We systematically contrast the broad, non-canonical scalar states—the $f_0(500)$ in $\pi\pi$ scattering and $K_0^*(700)$ in πK scattering—with their canonical vector counterparts, the $\rho(770)$ and $K^*(892)$. While the unusual scattering line shapes of the $f_0(500)$ and $K_0^*(700)$ are conventionally attributed to strong backgrounds and subthreshold Adler zeros [5,6], we demonstrate that their complex-pole properties, along with the narrow $\Delta(1232)$ nucleon resonance, are inherently unified through a single, well-defined threshold-pole topology.

2. Theoretical framework

We adopt the single resonance scattering matrix parametrization from Refs. [3,4], valid in the proximity of the resonance pole, assume an elastic resonance, and impose S-matrix unitarity. In that case, the complex phase of the scattering amplitude is given by the phase shift

$$\delta = \arctan \frac{\Gamma/2}{M - E} + \delta_B, \tag{1}$$

with the approximately constant background term δ_B. Here, E is center of mass energy. The interplay between broad resonances and their background in $\pi\pi$ and πK scattering has been extensively explored using similar constant-background models [7–10].

Up to this point, this may seem like the textbook Breit-Wigner parametrization. However, the key contribution from Refs. [3,4] is that for elastic resonances $\theta = 2\delta_B$, and $\delta_B = \delta_0$, where the kinematic baseline phase δ_0 is defined as

$$\delta_0 = -\arctan \frac{\Gamma/2}{M - E_0}. \tag{2}$$

* Corresponding author.
E-mail address: sasa.ceci@irb.hr (S. Ceci).

https://doi.org/10.1016/j.physletb.2026.140892
Received 20 May 2026; Received in revised form 10 July 2026; Accepted 24 August 2026
Available online 26 August 2026
0370-2693/© 2026 The Author(s). Published by Elsevier B.V. Funded by SCOAP³. This is an open access article under the CC BY license (http://creativecommons.org/licenses/by/4.0/).

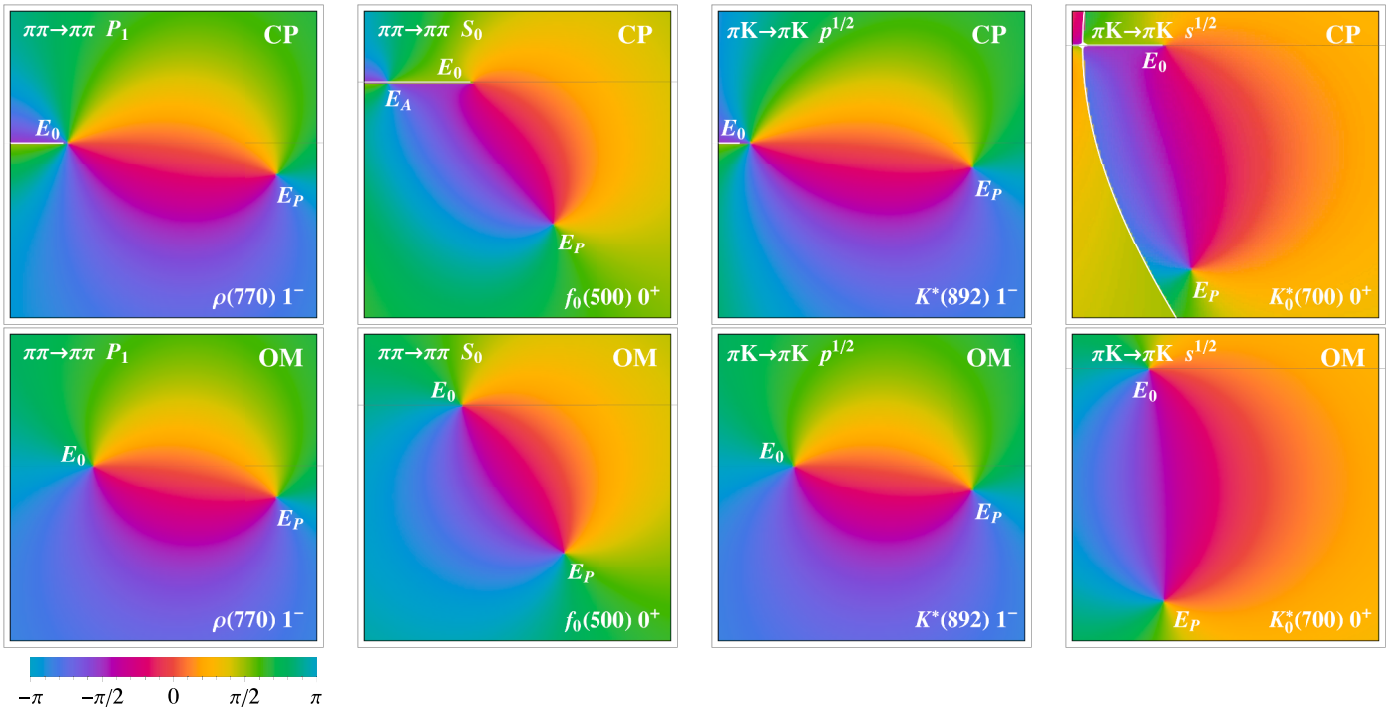


Fig. 1. Scattering amplitude phase ($\arg T$) in the complex energy plane. (Upper half) Amplitude is built from naturally expanded theoretical δ from Refs. [11,12] into the complex energy plane (CP). Here, E_0 is the threshold and E_P is the pole position. Adler zero (E_A) is clearly seen for $f_0(500)$, while for $K_0^*(700)$ it is obscured by the conformal variable cut structure. (Lower half) Amplitude constructed from the fitted δ in our model (OM). The poles E_P are clearly visible, while the thresholds E_0 are effectively described as simple zeros. The main goal of this figure is to be illustrative, therefore we removed the axis labels to avoid clutter. On the horizontal axis is the real part of the energy, on vertical is the imaginary part. Threshold for $\pi\pi$ is at 279 MeV, for πK is 636 MeV, and all pole positions are given in Table 1.

Here, E_0 is the elastic threshold energy. The geometrical meaning of the δ_0 is the angle between the real axis and the pole position seen from the threshold.

This framework assumes that the background phase δ_B, as well as the pole parameters M and Γ, are locally constant. While Γ and δ_B are naturally energy-dependent in fully dynamical models, locally assuming their constancy yields the exact elastic residue phase $\theta = 2\,\delta_B$ [13].

While the interplay between pole positions, background contributions, and elastic unitarity has been extensively studied globally through factorized S-matrix approaches like the Peking University (PKU) representation [14–17], our framework demonstrates that these fundamental relations manifest highly locally, driven predominantly by simple threshold topology.

It is important to emphasize that this framework serves as a rigorous test of single-channel elastic unitarity. While our general baseline mechanism was recently validated across 25 distinct N^* and Δ resonances in a comprehensive baryon framework [3,4], the current sample isolates the lightest canonical and non-canonical elastic mesons to test the boundaries of this constraint. Consequently, states like the $a_0(980)$ and $f_0(980)$ are excluded, as they reside in the immediate vicinity of the $K\bar{K}$ threshold and are inherently coupled-channel phenomena. Analyzing them requires the inelastic (and multi-resonance for $f_0(980)$) formalism developed in our previous works, which falls outside the scope of the strict elastic unitarity limit being tested here.

To test our hypotheses, we generate theoretical data points for δ using the parametrizations from Refs. [11,12,18]. We search for the poles and residues of scattering amplitude and we reconstruct it in the complex plane (CP) in the upper half of Fig. 1, using relation $T = (\cot\delta - i)^{-1}$.

3. Phase conversion

A persistent challenge in evaluating resonance parameters is the apparent discrepancy between the unitary residue phase θ extracted in the complex-energy plane and the bare coupling phase ϕ_g reported by high-precision dispersive analyses [11,12,19]. By consistently adopting the baryon resonance convention for the residue limit, $\lim_{E\to E_p}(E_p - E)\,T(E)$, we show that this discrepancy is essentially a kinematic artifact.

The phase θ is universally linked to the phase ϕ_g via the exact relation:

$$\theta = 2\phi_g - 2\arg(E_p) + (2l+1)\arg(q(E_p)), \tag{3}$$

where $q(E_p)$ is the momentum evaluated at the pole energy E_p, and l is the angular momentum number.

This translation absorbs both the Jacobian rotation from the Mandelstam s-plane to the E-plane and the complex centrifugal barrier kinematics. When this translation is applied, the apparent offset vanishes, and our threshold-derived phases exhibit striking agreement with results from the literature (cf. Table 1).

Higher-Order Derivative Diagnostics.—To distinguish genuine resonance poles from dynamically generated structures without relying on deep complex-plane extrapolation (CP), we introduce a diagnostic test based on higher-order energy derivatives of the phase shift [20]. Extending the traditional first-derivative time-delay methods [13,21], we exploit the property that for a generic Breit-Wigner resonance with a locally constant background δ_B, all even-order energy derivatives $\delta^{(2n)}(E)$ of Eq. (1) must cross zero at the resonance pole mass $\delta^{(2n)}(M_{2n}) = 0$. The corresponding widths are extracted analytically:

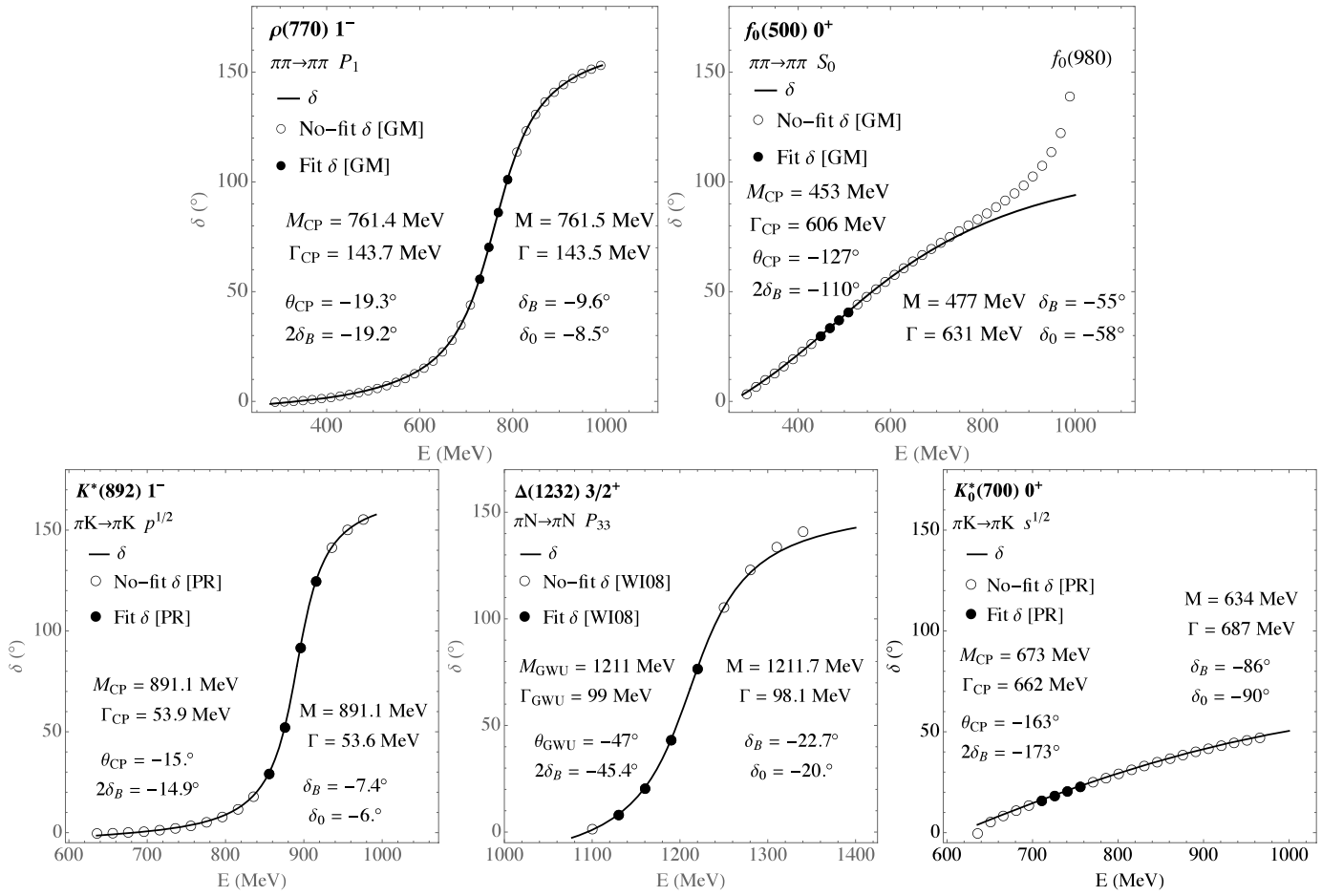


Fig. 2. Fitting our three-parameter model (OM) from Eq. (1) to the phase shifts from Refs. [11,12,18]. Only the four black circle data points at each graph are fitted. For comparison we show the pole parameters directly calculated at the pole position in the complex plane (CP). Since a mathematical model is used to generate the data, the χ^2_R has no statistically relevant value. Note how Δ(1232) stands half-way from Breit-Wigner to non-Breit-Wigner resonance and, as a Rosetta stone of a kind, possesses the features of both worlds (nice resonant shape, but also large background and significant residue phase).

$$\Gamma_{2n} = 2 \lim_{E \to M_{2n}} \sqrt[2n+1]{(-1)^{n-1}(2n)! \frac{M_{2n} - E}{\delta^{(2n)}(E)}}. \tag{4}$$

The residue phase is then unambiguously evaluated as $\theta_{2n} = 2\,\delta(M_{2n}) - 180°$.

We stress that this method is exclusively a theoretical post-processing tool designed for analytically continued, smooth dispersive phase shifts (such as those output by Roy-Steiner equations or L+P analytic continuations). Higher-order derivatives inherently amplify statistical noise, meaning this diagnostic is mathematically unsuitable for raw experimental data and requires the high numerical stability provided by established theoretical parametrizations.

For genuine, isolated poles, the extracted parameters for the lowest few even derivatives converge ($M_2 \approx M_4$ and $\Gamma_2 \approx \Gamma_4$). Conversely, the presence of hidden dynamics or nearby singularities—such as subthreshold Adler zeros—breaks this local analytic symmetry, causing the higher-order extractions to explicitly diverge. As shown in Table 1, the canonical vectors $\rho(770)$ and $K^*(892)$ exhibit perfect second-to-fourth derivative (D2/D4) convergence. In stark contrast, the $f_0(500)$ parameters shift systematically, providing a clear, extrapolation-free fingerprint of the non-local dynamical effects dominating the scalar sector. For $K_0^*(700)$, due to its closeness to the threshold, there is no resonant signal even in the first derivative, let alone the higher ones.

4. Fitting the constructed data

We construct the elastic scattering amplitude T from the phase shifts and search for the pole positions and their residues directly in the complex energy plane (CP). This convention (pole in E, rather than Mandelstam s) is standard in baryon spectroscopy. We adopt it here to establish a unified framework for distinct types of hadrons, noting that its application remains robust even for highly relativistic, broad states, since many well-established baryon resonances exhibit widths comparable to, or even exceeding those of the light scalar mesons.

The near-resonance region is isolated by fitting Eq. (1) to sliding windows of four consecutive theoretical data points, selecting the local parametrization that minimizes χ^2. This procedure ensures a stable extraction of M, Γ, and δ_B, even for broad resonances where the background variation is non-negligible farther away from the pole. The fit results comparing our model (OM) to the constructed data are shown in Fig. 2.

Our analysis of the vector sector ($\rho(770)$ and $K^*(892)$) shows nearly perfect agreement between OM fits and CP values. For these states, the extrapolated fitting curve covers the entire elastic range, and the residue phase θ is accurately predicted by $2\delta_B$, validating the constant-background approximation even in the presence of a dominant centrifugal barrier.

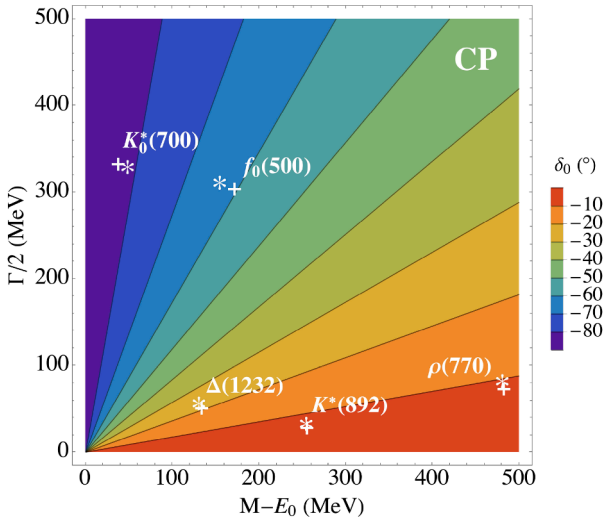


Fig. 3. Phase rotation plot showcasing the kinematic consistency across different hadronic sectors. It is crucial to note that the markers represent entirely independent dispersive data from the literature, not the output of our model. Each "+" denotes the pole position ($M - E_0$, $\Gamma/2$) extracted from established dispersive analyses (CP). The "∗" indicates the position if the baseline phase δ_0 were replaced by the actual, independently extracted dispersive phase $\theta/2$. The proximity of "+" and "∗" symbols across $\pi\pi$, πK, and πN sectors is a strong physical correlation demonstrating that the residue phase is primarily driven by the threshold kinematics.

In the scalar sector ($f_0(500)$ and $K_0^*(700)$), we observe a stable OM fit despite the non-resonant phase shift shapes. The 25 MeV mass discrepancy and the 10°–15° phase drift from CP values are systematic. This identifies the limit where our baseline model meets chiral dynamics.

A straightforward way to enforce the Adler zero would be to explicitly multiply the local amplitude by an unbounded polynomial factor $(E - E_A)$. However, doing so directly in the numerator fundamentally violates elastic unitarity ($\mathrm{Im}\, T = |T|^2$) and destroys the required asymptotic behavior. To preserve asymptotic limits and attempt to maintain elastic unitarity, one would be forced to introduce at least one additional, arbitrary pole into the denominator, completely negating the parameter-free simplicity of our framework. In rigorous dispersive representations, such chiral zeros are implemented within the inverse amplitude (e.g., via $\cot\delta$). In a fully unitary amplitude, the massive phase rotation generated by the subthreshold zero is heavily compensated by the complex branch cut structure at the threshold. Our constant-background model acts as a local effective theory: it naturally absorbs the net local effect of this compensated structure (cut plus zero) into a single effective zero in close proximity to the threshold, leaving the 10°–15° deviation as the quantitative measure of the uncompensated chiral residual.

We note that $f_0(500)$ and $K_0^*(700)$ share an intriguing feature with the relatively narrow $\Delta(1232)$ πN elastic resonance: all three are unusually close to their thresholds. Despite being substantially narrower, the $\Delta(1232)$ has a residue phase more than double that of the $\rho(770)$. This strongly suggests that the kinematic angle δ_0, and not the width alone, dictates the phase. All our results are collected in Table 1.

To further test our results, we apply the L+P method, which has successfully been used in nucleon spectroscopy for extractions of the pole and residue properties [22]. In addition to Laurent part handling the poles, it uses Pietarinen expansion with conformal variable taking care of channel openings. The L+P results are fully consistent with ours, which suggests that Adler zeros are effectively subsumed within the local behavior of the data. In addition, it means that L+P should be modified for scalar mesons to include Adler zeros in order to precisely extract properties of the dynamical poles.

Table 1
The results of fitting our model (OM) to the phase shifts from Refs. [11,12]. We write $2\delta_0$ and $2\delta_B$ for easier comparison with phase shift θ. The L+P method [22] is used on scattering amplitude constructed from the phase shifts. D2/D4 is a derivative method we propose for distinguishing genuine from dynamical poles (if $D2 \neq D4$, there is hidden dynamics). CP results are evaluated at the pole position in the complex plane. PR, GM and GWU are results of the original analyses from Refs. [11,12,18]. HR is from Ref. [19], and PDG estimates are from Ref. [2].

State	Src.	M (MeV)	Γ (MeV)	$2\delta_B \mid \theta$ (°)	$2\delta_0$ (°)
$K^*(892)$	OM	891.1	53.6	−14.9	−12.0
	L+P	891.0	53.7	−15.0	−12.0
	D2	891.1	53.9	−14.8	−12.0
	D4	891.1	53.9	−14.9	−12.0
	CP	891.1	53.9	−15.0	−12.0
	PR	890 ± 2	51.6 ± 2.4	-15.2 ± 1.2	−11.6
	PDG	890 ± 14	52 ± 12	− − −	-11.7 ± 2.8
$\rho(770)$	OM	761.5	143.5	−19.2	−16.9
	L+P	761.3	143.3	−19.4	−16.9
	D2	761.5	143.7	−19.2	−16.9
	D4	761.4	143.7	−19.2	−16.9
	CP	761.4	143.7	−19.3	−16.9
	GM	$763.7^{+1.7}_{-1.5}$	$146.4^{+2}_{-2.2}$	-18.6 ± 1.0	−17.2
	HR	760.6 ± 0.8	142.4 ± 0.9	-19.0 ± 0.6	−16.8
	PDG	763 ± 2	145 ± 3	− − −	-17.0 ± 0.4
$\Delta(1232)$	OM	1212	98	−45	−40
	L+P	1211	98	−46	−40
	GWU	1211	99	−47	−41
	PDG	1210 ± 1	100 ± 2	-46^{+1}_{-2}	-41 ± 2
$f_0(500)$	OM	474	629	−110	−116
	L+P	485	618	−107	−113
	D2	477	627	−110	−116
	D4	461	578	−116	−116
	CP	453	606	−127	−120
	GM	457^{+14}_{-13}	558^{+22}_{-14}	-118 ± 12	−115
	HR	449 ± 6	550 ± 24	-124 ± 10	−117
	PDG	400–550	400–700	− − −	-109 ± 25
$K_0^*(700)$	OM	634	687	−173	−181
	L+P	637	674	−171	−180
	D2/4	Not seen			
	CP	673	662	−163	−167
	PR	648 ± 7	560 ± 32	-180 ± 8	−175
	PDG	630–730	520–680	− − −	-163 ± 19

Indeed, when we compare the fits of our model (OM) and L+P, and the relevant results from the literature [11,12,19], which we had to translate to the nucleon resonance convention using Eq. (3), the agreement in the residue phases seems striking.

The systematic drift observed in the scalar sector is not a failure of our baseline model but a clear identification of dynamical contributions. While the pole-threshold topology provides the "skeleton" of the residue phase (accounting for over 85% of its value), the Adler zero, required by chiral symmetry, adds a well-defined correction. This confirms our previous thesis [3,4] that residue phases are largely fixed by unitarity, with the remaining physics residing in the precise pole placement and subtle dynamical shifts.

The CP results further confirm our main assumption—that the main driving term of the residue phase θ is our kinematic baseline $2\delta_0$. To see that more clearly, in Fig. 3 we show a combined plot of independent, externally calculated CP results. The straight rays from the origin represent our theoretical kinematic baseline δ_0. The points mapped onto this plane, however, are not outputs of our model: the cross signs denote the pole positions extracted from established independent dispersive analyses, and the asterisks denote where these exact poles would lie if their angle was given by the independently extracted true dispersive

phase $\theta/2$. The difference is surprisingly small even for the $f_0(500)$ and $K_0^*(700)$.

The kinematic origin of the residue phase is robust, but not completely rigid. As formally demonstrated by our D2/D4 diagnostics (Table 1), the subtle deviations observed in the scalar sector act as a direct quantitative measure of the underlying chiral dynamics. Future extensions of this framework to heavier scalar states, such as the $f_0(980)$ and $K_0^*(1430)$, could potentially yield further insights into their underlying quark substructure, complementing existing large-N_c analyses [23].

5. Conclusion

The fact that the simple pole plus constant background fits almost perfectly various theoretical elastic phase shifts for $\pi\pi$, πK, and πN scattering [11,12,18] tells us that this is a reasonable approximation quite far in the complex plane. That means the constant background δ_B can do the heavy lifting of setting both the scattering amplitude to zero at the threshold (where the total phase shift δ will be zero), setting its imaginary part to unity at the Breit-Wigner peak position (where δ is 90°), and setting the residue phase to $\theta = 2\delta_B$ at the pole position. Consequently, the value of the background phase shift is to a significant extent given by the kinematic baseline δ_0, defined as the angle between the pole position and the real energy axis seen from the threshold. This has been suggested by imposing the S-matrix unitarity on the elastic scattering amplitudes from Refs. [3,4]. There, it was shown that such amplitude is in fact a mathematical identity valid when there are no additional singularities or zeros between the threshold and the pole. Indeed, we have seen the strongest departure of δ_B from δ_0 for the spin-0 partial waves where an Adler zero is present in the proximity of the threshold. Finally, our main hypothesis is once more confirmed by naturally expanding the theoretical phase shifts from the literature into the complex plane, and finding that $\theta/2$ and δ_0 are almost indistinguishable. The anomalous nature of the $f_0(500)$ and $K_0^*(700)$ states is thus clarified: their extreme pole locations mandate a maximal kinematic angle δ_0, effectively detaching the Breit-Wigner peak from the pole mass while dictating a nearly constant background phase across the entire elastic domain.

Declaration of competing interest

The authors declare that they have no known competing financial interests or personal relationships that could have appeared to influence the work reported in this paper.

Data availability

The data that support the findings of this study are openly available in Zenodo [24] of this work.

Supplementary material

Supplementary material associated with this article can be found in the online version at 10.1016/j.physletb.2026.140892.

References

[1] R.H. Dalitz, R.G. Moorhouse, Proc. R. Soc. Lond. A 318 (1970) 279.
[2] S. Navas, et al., [Particle Data Group], Review of particle physics, Phys. Rev. D 110 (2024) 030001.
[3] S. Ceci, R. Omerović, H. Osmanović, M. Uroić, B. Zauner, Phys. Lett. B 872 (2026) 140136.
[4] S. Ceci, R. Omerović, H. Osmanović, M. Uroić, M. Vuksić, B. Zauner, Phys. Lett. B 875 (2026) 140332.
[5] S.L. Adler, Phys. Rev. 137 (1965) B1022.
[6] J.R. Peláez, Phys. Rep. 658 (2016) 1.
[7] M. Harada, F. Sannino, J. Schechter, Phys. Rev. D 54 (1996) 1991.
[8] M. Harada, F. Sannino, J. Schechter, Phys. Rev. Lett. 78 (1997) 1603.
[9] D. Black, A.H. Fariborz, F. Sannino, J. Schechter, Phys. Rev. D 58 (1998) 054012.
[10] A.H. Fariborz, J. Ho, T.G. Steele, Phys. Rev. D 111 (2025) 094023.
[11] J.R. Peláez, A. Rodas, Phys. Reps. 969 (2022) 1.
[12] R. García-Martín, R. Kamiński, J.R. Peláéz, J. Ruiz de Elvira, F.J. Ynduráin, Phys. Rev. D 83 (2011) 074004.
[13] G. Höhler, Landolt-Börnstein: Numerical Data and Functional Relationships in Science and Technology. Group 1, Vol. 9, Subvolume b, Part 2, 202, Springer-Verlag, 1983.
[14] Z. Xiao, H.Q. Zheng, Nucl. Phys. A 695 (2001) 273.
[15] H.Q. Zheng, Z.Y. Zhou, G.Y. Qin, Z. Xiao, J.J. Wang, N. Wu, Nucl. Phys. A 733 (2004) 235.
[16] Z.Y. Zhou, G.Y. Qin, P. Zhang, Z.G. Xiao, H.Q. Zheng, N. Wu, JHEP 02 (2004) 043.
[17] Z.Y. Zhou, H.Q. Zheng, Nucl. Phys. A 775 (2006) 212.
[18] R.A. Arndt, W.J. Briscoe, I.I. Strakovsky, R.L. Workman, Phys. Rev. C 74 (2006) 045205.
[19] M. Hoferichter, J. Ruiz de Elvira, B. Kubis, U.-G. Meißner, Phys. Lett. B 853 (2024) 138698.
[20] S. Ceci, J. Stahov, A. Svarc, S. Watson, B. Zauner, Phys. Rev. D 77 (2008) 116007.
[21] E.P. Wigner, Phys. Rev. 98 (1955) 145.
[22] A. Svarc, M. Hadzimehmedović, R. Omerović, H. Osmanović, J. Stahov, Phys. Rev. C 89 (2014) 045205.
[23] J.R. Peláez, Phys. Rev. Lett. 92 (2004) 102001.
[24] S. Ceci, Data used in the paper: elastic phase shift analysis reveals the geometric origin of the residue phase, 2026, [dataset] Zenodo, https://doi.org/10.5281/zenodo.19258981